Surface & Coatings Technology 206 (2012) 3650–3657

Contents lists available at SciVerse ScienceDirect

Surface & Coatings Technology

journal homepage: www.elsevier.com/locate/surfcoat

Optical and structural properties of Nb_2O_5–SiO_2 mixtures in thin films

Vesna Janicki [a,*], Jordi Sancho-Parramon [a,b], Sergiy Yulin [c], Marcel Flemming [d], Andrey Chuvilin [d,1]

[a] Ruđer Bošković Institute, Bijenička c. 54, 10000 Zagreb, Croatia
[b] Departament de Fisica Aplicada i Optica, Univeristat de Barcelona, Marti i Franques 1, 08028, Barcelona, Spain
[c] Fraunhofer-Institut für Angewandte Optik und Feinmechanik IOF, Albert-Einstein Str. 7, 07745 Jena, Germany
[d] University of Ulm, Albert Einstein Allee 11, 89069 Ulm, Germany

ARTICLE INFO

Article history:
Received 23 March 2011
Accepted in revised form 4 March 2012
Available online 12 March 2012

Keywords:
Optical characterization
Optical properties
Structural properties
Material mixture
Effective medium theory

ABSTRACT

Mixed material thin films are used in gradient index optical systems **as** their refractive index can be tailored to meet requirements. For the system to meet the optical performance requirements, it is necessary to relate the refractive index profile of the design to the volume fraction of the components of the mixture. Here we report that for electron-beam co-deposited Nb_2O_5–SiO_2 mixtures, the most appropriate effective medium theory is Lorentz–Lorenz theory. The optical properties of a mixture are related to the structure of the composite. The structural properties of the mixtures studied justify the appropriateness of Lorentz–Lorenz theory for this kind of effective medium.

1. Introduction

Optical thin film coatings with refractive index changed continuously as a function of the depth of the layer are known as gradient index films or inhomogeneous films. Gradient index systems can be advantageous in terms of optical performance and mechanical properties compared to conventional HL-stack designs with alternating layers of materials of high and low refractive index. Excellent theoretical work on the optical behaviour of gradient index films has been published over recent decades [1–3]. Additional advantages that can be expected from inhomogeneous coatings are low stress, tribological resistance [4–6] and higher laser induced damage thresholds [7] than those of classical multilayer stacks.

In order to obtain the desired design and optical performance, it is necessary to calculate the optical constants of the material mixture that is used in the design and later deposited. The optical constants can be calculated using different mixing models. These models relate the optical constants of a mixture of given composition with the optical constants of the pure materials. Several models, known as effective medium theories (EMTs), have been proposed: Bruggeman [8], Lorentz-Lorenz [9], Maxwell Garnett [10] and a linear combination of refractive indices [11]. The EMTs that are appropriate for the material mixture deposited by the given technique should be applied for optical characterisation, as well as during design.

In this study, we assess the appropriateness of the Lorentz–Lorenz model for calculating the refractive index of Nb_2O_5–SiO_2 mixtures during optical characterisation, and therefore the necessity to introduce it into the design software [11,12]. Samples of different mixtures of SiO_2 and Nb_2O_5 with a constant refractive index throughout the layer were deposited in order to establish which EMT best describes Nb_2O_5–SiO_2 mixtures.

The appropriateness of the Lorentz–Lorenz model was related to the structure of the mixtures by additional measurements: FTIR (Fourier transform infrared) spectroscopy, TEM (transmission electron microscopy), XRD (X-ray diffraction) and AFM (atomic force microscopy). In order to verify the correlation of the structure with the results of the optical characterisation, the samples were annealed; upon thermal treatment, phases are expected to separate and the optical properties to follow the Bruggeman or Maxwell-Garnett law, which are the most appropriate for this kind of mixtures.

2. Theory

In this section we present an overview of the material properties necessary to understand the experimental results of our work. Also, a brief description of EMTs is given to explain their suitability for the mixtures studied.

2.1. Materials

SiO_2 films are amorphous, having compressive stress. Crystallisation occurs upon thermal treatment at temperatures above 1100 °C. The characteristic bonds of fused silica that are detectable by infrared

* Corresponding author. Tel.: +385 1 4571247; fax: +385 1 4680108.
E-mail address: janicki@irb.hr (V. Janicki).
[1] Present address: CIC nanoGUNE Consolider, Av. de Tolosa 76, 20018, San Sebastian, Spain and IKERBASQUE, Basque Foundation for Science, 48011, Bilbao, Spain.

0257-8972/$ – see front matter © 2012 Elsevier B.V. All rights reserved.
doi:10.1016/j.surfcoat.2012.03.015

spectroscopy are at [13]: 1220 cm^{-1}, 1080 cm^{-1}, 800 cm^{-1} and 460 cm^{-1}.

Deposited Nb_2O_5 films are mainly amorphous and do not crystallize easily. Coatings are wear resistant and fairly hard. For pure Nb_2O_5, onset of crystallisation is between 400 °C and 500 °C [14–16] resulting in a hexagonal structure (Powder Diffraction File [17]: card No. 28–0317) while at temperatures between 600 °C and 700 °C, it adopts an orthorhombic structure (Powder Diffraction File [17]: card No. 30-0873 or 27-1003) [16]. A characteristic feature of pure Nb_2O_5 infrared spectra is the absorption band around 600 cm^{-1}, which corresponds to the Nb–O bonds of slightly distorted NbO_6 octahedra [16]. This band increases with increasing temperature, splits and shifts to a lower frequency, which suggests the existence of different Nb–O species or inequivalent Nb–O groups. The band at 850 cm^{-1} corresponds to Nb–O–Nb stretching [18].

SiO_2 has been reported to stabilize amorphous Nb_2O_5 [19]. Nb_2O_5 crystallisation is known to vary according to the interactions between the compounds it encounters. The structure of pure Nb_2O_5 is therefore very different from that of the systems it forms with other species. The interactions between Nb_2O_5 and other materials affect its stability and, consequently, the final structure. When a strong interaction is established via Si–O–Nb linkages, the superficial Nb_2O_5 presents only the amorphous phase after thermal treatment at 500 °C for 2 h [19]. Even after 48 h of treatment at 1000 °C, only weak diffraction peaks were attributed to the hexagonal phase. The interactions between Nb_2O_5 and SiO_2 are responsible for Nb_2O_5 stabilisation, as they reduce Nb_2O_5 mobility thus preventing crystallisation. It has been shown that a strong interaction between SiO_2 and Nb_2O_5 is established during the sol–gel process, i.e. it involves the formation of Si–O–Nb bonds [19]. This conclusion is based on observation of the infrared band between 930 cm^{-1} and 920 cm^{-1} that disappears with the agglomeration process after high-temperature treatment.

2.2. Effective medium theories

Typically, when considering mixtures of materials, it is assumed that each material is present as a phase with a microstructure that is large enough to exhibit the same optical properties as a layer of that material, but small in comparison to the wavelength of the incident light. In this way the medium is microscopically heterogeneous, but macroscopically homogeneous. To fulfil this condition for the visible and up to mid-infrared wavelengths, the microstructure should typically have dimensions of 3–30 nm [20] (the shorter the wavelength, the lower the upper size limit).

EMTs were devised to describe properties of such effectively homogeneous media [21]. The most widely used are the Maxwell–Garnett [10] (MG), Bruggeman [8] (BG) and Lorentz–Lorenz [9] (LL) EMT. The equations for two-material mixtures are as follows:

$$\text{MG} \quad \frac{\varepsilon_{eff}-\varepsilon_H}{\varepsilon_{eff}+2\varepsilon_H} = (1-f_H)\frac{\varepsilon_L-\varepsilon_H}{\varepsilon_L+2\varepsilon_H} \tag{1}$$

$$\text{BG} \quad f_H\frac{\varepsilon_H-\varepsilon_{eff}}{\varepsilon_H+2\varepsilon_{eff}} + (1-f_H)\frac{\varepsilon_L-\varepsilon_{eff}}{\varepsilon_L+2\varepsilon_{eff}} = 0 \tag{2}$$

$$\text{LL} \quad \frac{\varepsilon_{eff}-1}{\varepsilon_{eff}+2} = f_H\frac{\varepsilon_H-1}{\varepsilon_H+2} + (1-f_H)\frac{\varepsilon_L-1}{\varepsilon_L+2} \tag{3}$$

where ε_{eff}, ε_H and ε_L are the effective dielectric functions of the mixture, high and low index materials, respectively. Volume fractions of high and low index material are f_H and f_L, where $f_H + f_L = 1$.

The first two theories assume that the mixed materials are in separate phases. MG considers a mixture that has two (or more) separate grain structures where particles of the first material are dispersed in a continuous host of the second material. The host in Eq. (1) is the high-index material. BG assumes an aggregate structure with random mixture of two (or more) material phases filling the space. In the limit of small volume fractions (f_v), the predictions of the two theories approach to each other. In the case of higher filling factors, i.e. when the volume fraction of one material is comparable to the volume fraction of the other, BG is valid to a smaller particle radius than MG [20]. LL takes the average molecular polarizability of the components. In this case no phase separation is considered as it is supposed that the mixture is at the atomic/molecular scale.

An additional simple model is the linear model (LIN), which considers linear dependence of the refractive index on the volume fractions of the constituents [9]:

$$\text{LIN} \quad \sqrt{\varepsilon_{eff}} = f_H\sqrt{\varepsilon_H} + (1-f_H)\sqrt{\varepsilon_L}. \tag{4}$$

3. Experimental details

3.1. Deposition of samples

A Leybold Syrus Pro 1100 deposition system was used for electron beam co-evaporation of Nb_2O_5 and SiO_2 to produce mixture coatings and gradient index films [22,23]. The chamber was equipped with two electron beam guns, two crucibles with evaporation materials and a plasma source. The deposition rates ($r(t)$) were measured by two quartz crystal monitors, one for each material. The concentrations of materials in the deposited layer, and therefore its refractive index, were controlled via the emission current of electron beam guns. The deposition rate of each material was kept constant during the production of each sample.

The deposition of the materials (Nb_2O_5 and SiO_2) was performed in an argon atmosphere as the working gas. Additionally, oxygen was employed as a reactive gas to maintain the stoichiometry of the evaporated materials. Typical basic pressure before the start of deposition was 4×10^{-7} mbar. Prior to deposition the substrates were heated in the deposition chamber to 150 °C, which was the working temperature. The substrates were cleaned first in an ultrasound bath and then by plasma etching for 3 minutes in the deposition chamber. To ensure uniformity of the film thickness across the substrate, the substrates were placed in the calotte rotating with the speed of approximately 20 rpm. The crucibles were set to rotate at 0.2 rpm to prevent deformation of the vapour cloud due to any decreased quantity of material in them during long processes. In each deposition process Suprasil and silicon wafer chunks were used as substrates.

Layers of constant mixed composition throughout their thickness, with different SiO_2 to Nb_2O_5 ratios were deposited to verify which EMT is best to characterise Nb_2O_5–SiO_2 mixtures. Five coatings were produced with a volume fraction of SiO_2 $f_v(SiO_2)$ ranging from approximately 0.2 to 0.8 in more or less equal steps. The deposition rates for the samples with: maximum (n_M), less than maximum (n_{M-x}), medium (n_{MED}), more than minimum (n_{m+x}) and minimum (n_m) content of Nb_2O_5 are shown in Table 1. The same table shows $f_v(SiO_2)$ and the expected thicknesses calculated from $r(t)$ recorded during deposition. The deposition time for all the samples was

Table 1
Set rates of deposition (r_{set}), $f_v(SiO_2)$ and thickness, d, of the mixture layers calculated from recorded rates of deposition.

Sample	$r_{set}(Nb_2O_5)/r_{set}(SiO_2)$ (nm/s)	$f_v(SiO_2)$ from $r(t)$	d from $r(t)$ (nm)
n_M	1.2/0.3	0.197	446.91
n_{M-x}	0.95/0.55	0.357	439.63
n_{MED}	0.75/0.75	0.486	439.76
n_{m+x}	0.55/0.95	0.615	428.10
n_m	0.3/1.2	0.784	429.02

310 s. The samples were post-annealed for 5 h in air at 500 °C and 750 °C.

3.2. Measurements

The reflectance and transmittance at 6° incidence in the range 350–950 nm were measured using a Perkin Elmer Lambda 900 spectrophotometer for the optical characterisation of the deposited samples. A VN-attachment allowing absolute measurement of reflectance without moving the sample after transmittance measurement was used. For the optical characterisation of the samples, general-purpose software [24] (NKDMatl) was used. By fitting the experimental spectra, the software determines the optimal value of a set of parameters that define the sample. The layers were represented as coatings of unknown thickness, *d*, and refractive index, *n*, following either the Tauc-Lorentz [25] or Cauchy [26] dispersion law. Fitting the optical characteristics of the model to the experimental data gives values of the optical parameters of the dispersion law applied and layer thickness.

FTIR measurements can detect the absorption band related to the presence of Si–O–Nb bonds, indicating the level of mixing of the two phases. The peaks show the dependence of band intensity on the concentration of the bonds and Nb_2O_5, and the annealing temperature. The intensity of this band should decrease, while that of the band associated with Si–O–Si bonds should increase, as a function of temperature, as this indicates separation into phases. A BIO-RAD model FTS 175 FTIR spectrometer was used to take the FTIR measurements. The spectra were measured in the wavenumber range 400–7000 cm^{-1}. XRD can also show the level of mixing of SiO_2 and Nb_2O_5. If no diffraction peaks are detected, the mixture is amorphous or crystallites are very small (less than 2–3 nm) [27]. In this case, the phases cannot be distinguished. The presence of diffraction peaks indicates crystallinity in the coating and separation of the materials into phases. XRD was performed using a Burker D505 diffractometer with Cu-Kα radiation at 0.154 nm, applying the large angle X-ray diffraction method. The samples deposited on Suprasil substrates were subjected to XRD analysis. The measurements were performed in the range of angles 7.5°–30°. AFM was used to detect crystalline grains formed on the layer surface after thermal treatment. The samples were measured at different scan sizes (1 μm × 1 μm and 10 μm × 10 μm). All the measurements were performed at IOF, Jena, Germany. Selected area electron diffractions (SAED) obtained using TEM can confirm the level of crystallisation found by XRD. Conventional TEM, high resolution TEM (HRTEM) and Z-contrast STEM (HAADF STEM) images can illustrate the structure of the layer in terms of the distribution of materials and grains, demonstrating again restructuring of the materials and separation into phases. The TEM study was performed using a Titan 80–300 TEM at the University of Ulm, Germany.

4. Results

4.1. Optical characterisation

The five mixture layers deposited on Suprasil were measured AD and after five hours of annealing in air at 500 °C and 750 °C. The sample with a pure Nb_2O_5 layer was treated in the same way. The sample with a pure SiO_2 layer was not annealed since the structural changes in this material were only expected at higher temperatures. Upon annealing at 750 °C, the Nb_2O_5 sample as checked by the naked eye showed milky reflection typical of high scattering, which indicates crystallisation in the layer. Therefore, optical characterisation could not be performed. For this reason, scattering measurements were performed for Nb_2O_5 and other annealed high content Nb_2O_5 samples using a Perkin Elmer Lambda 19 spectrometer with an Ulbricht integrating sphere. No significant scattering (S) was detected for any of the samples annealed at 500 °C. Scattering spectra for samples annealed at 750 °C are presented in Fig. 1. The peaks in the spectra of Nb_2O_5 and n_M samples (Fig. 1) correspond to peaks in reflectance spectra (not shown): the more light is reflected, the more light is scattered. There is no significant absorption in the range 350–950 nm for AD or 400–950 nm for the annealed samples. The results of optical characterisation, using Tauc-Lorentz (TL) or Cauchy (C) model with exponential absorption, are shown in Table 2. The samples showing scattering were rotated 90° and their reflectance was measured again. No anisotropy was found in this way. Optical characterization did not show significant inhomogeneities of the refractive index through the thickness of the layers. The dispersions of the refractive indices are presented in Fig. 2.

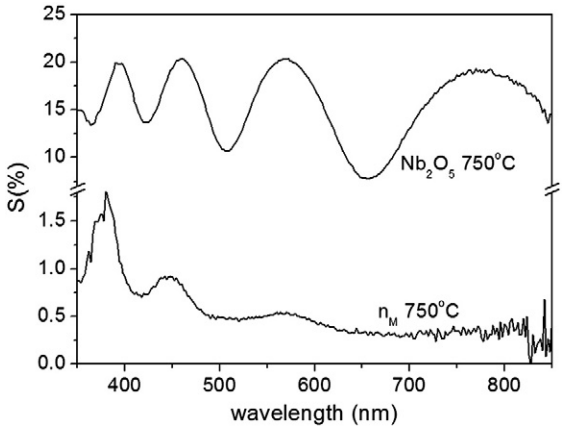

Fig. 1. Scattering of the annealed high content Nb_2O_5 samples prepared on Suprasil substrate.

4.2. FTIR

Before each FTIR measurement was taken, a Si substrate spectrum was taken as background, so the data presented in Figs. 3 and 4 are solely spectra of the deposited layers. Fig. 3 shows absorption curves of AD and annealed samples in the range where Si–O–Si, Nb–O and Si–O–Nb bands are expected. Fig. 4 shows FTIR spectra in the range where a water absorption band is expected [28]. The absorbance, *A*, is obtained from measurement of the sample and A_{sub} from measurement of the bare Si substrate. The measurements were taken 7 days after deposition, when no further water absorption was detected.

Table 2
Results of optical characterisation of AD and annealed mixture samples.

		n at 570 nm	*d* (nm)	model
Nb_2O_5	AD	2.284	450.3	TL
	500 °C	2.313	436.7	TL
n_M	AD	2.086	449.6	TL
	500 °C	2.104	433.5	TL
	750 °C	2.186	404.2	C
n_{M-x}	AD	1.903	506.8	C
	500 °C	1.920	481.2	C
	750 °C	1.993	442.9	C
n_{MED}	AD	1.839	464.0	C
	500 °C	1.840	441.1	C
	750 °C	1.892	415.3	C
n_{m+x}	AD	1.707	500.6	C
	500 °C	1.714	473.9	C
	750 °C	1.746	430.0	C
n_m	AD	1.600	471.7	C
	500 °C	1.597	453.8	C
	750 °C	1.599	421.6	C
SiO_2	AD	1.467	507.3	C

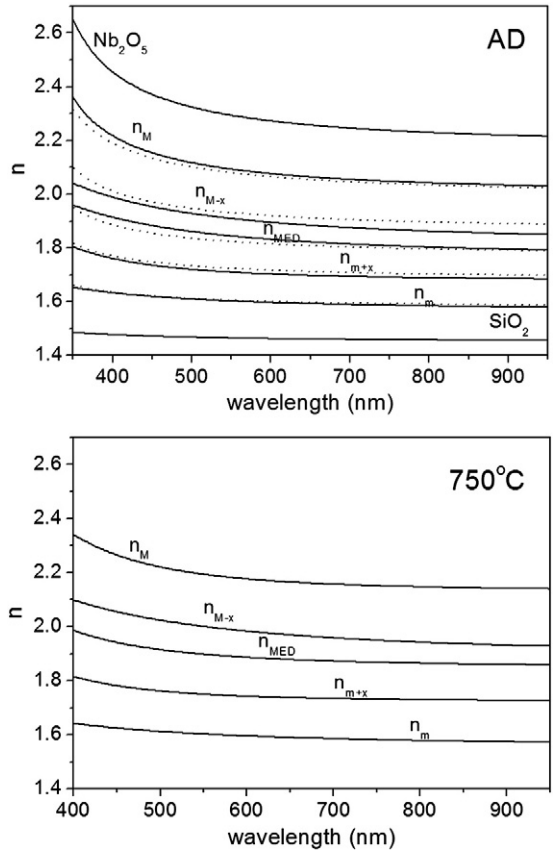

Fig. 2. Refractive index dispersions of the mixture samples, AD and annealed at 750 °C. Theoretical LL dispersion curves for the corresponding AD samples are presented with dots.

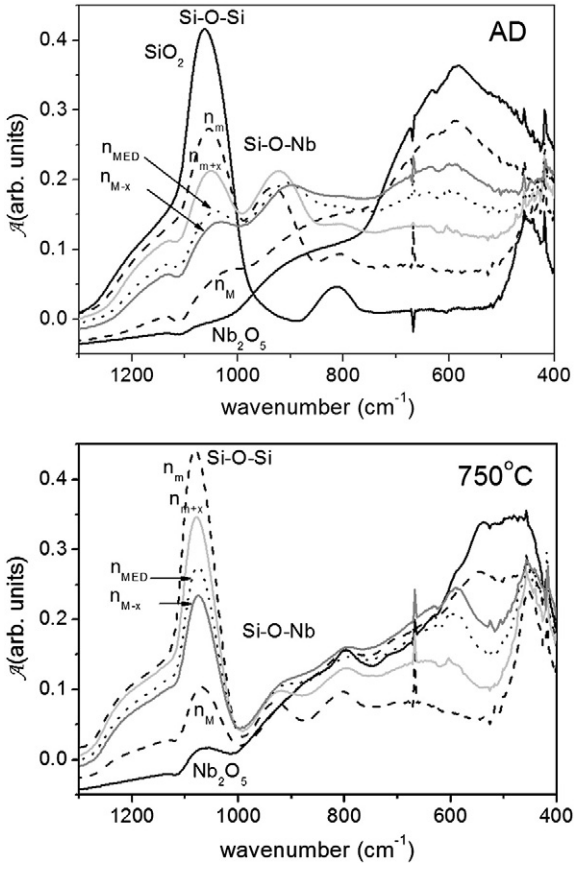

Fig. 3. FTIR spectra of AD and annealed mixture samples deposited on silicon wafer chunks.

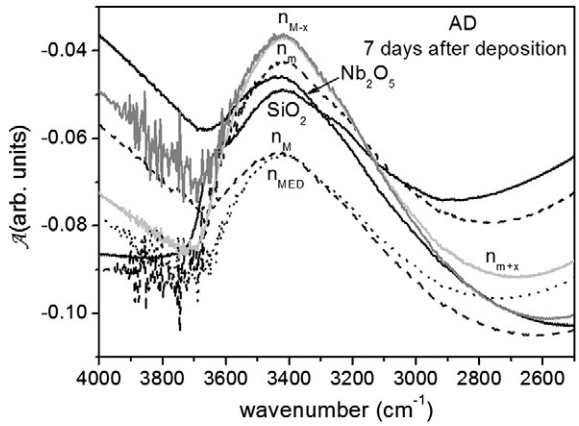

Fig. 4. Water absorption band of the mixture samples deposited on silicon wafer chunks.

4.3. XRD

The small angle X-ray reflection (SAXR) and the large angle X-ray diffraction (LAXD) measurements were performed in Bragg-Brentano geometry (Θ–2Θ) using CuKa radiation (λ = 0.154 nm). The LAXD measurements are shown in Fig. 5. The peaks correspond to hexagonal and orthorhombic crystalline structures of Nb_2O_5. The values of root mean square (RMS) surface roughness obtained from these measurements, as for the density of the samples, are presented in Table 3. Also, the density of the layers was determined from approximately 100 nm top thickness of the film.

4.4. AFM

The AFM topographs of AD and annealed Nb_2O_5, and of n_M layers deposited on Suprasil are shown in Figs. 6 and 7. The average roughness values obtained from several AFM measurements are given in Table 3 and compared with values obtained from XRD.

4.5. TEM

Selected area electron diffraction (SAED) and TEM images of n_M sample, AD and annealed at 750 °C, deposited on Si are shown in Figs. 8 and 9, respectively. A high angle annular dark field scanning TEM (HAADF STEM) image is also presented. SAED patterns include crystalline reflections of Si substrate as internal calibration standard.

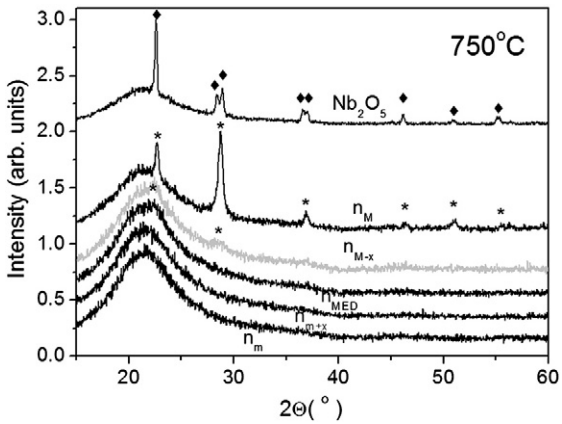

Fig. 5. LAXD spectra of samples prepared on Suprasil substrates annealed at 750 °C. Crystallization was observed for the three samples with the highest content of Nb_2O_5 annealed at 750 °C. Peaks characteristic of a hexagonal structure are denoted by * and those characteristic of an orthorhombic structure by ◆.

Table 3
Comparison of roughness values obtained from AFM and XRD, density (ρ) of the layers obtained from XRD analysis.

Sample	Roughness AFM (nm)		Roughness XRD (nm)		ρ XRD (g/cm^3)	
	AD	750 °C	AD	750 °C	AD	750 °C
Nb_2O_5	0.94	11.96	1.7	3.3	4.5	4.5
n_M	1.03	1.24	1.8	1.6	4.3	4.4
n_{M-x}	–	–	2.0	1.3	3.65	4.0
n_{MED}	1.05	1.22	–	–	–	–
n_{m+x}	–	1.44	–	–	–	–
n_m	1.36	1.47	–	–	–	–
SiO_2	1.82	–	–	–	–	–

5. Discussion

Since the band gap for SiO_2 and Nb_2O_5 is around 8 eV (160 nm) and 3.3 eV (375 nm), respectively, for optical characterisation in the spectral range of interest the Cauchy model is appropriate for SiO_2 and low content Nb_2O_5 samples. The Tauc-Lorentz model is more appropriate for Nb_2O_5 and samples with a high content of this material. As mentioned before, due to significant scattering of the Nb_2O_5 sample annealed at 750 °C (Fig. 1), it could not be optically characterised. However, due to low scattering for the n_M sample, instead of Tauc-Lorentz, the Cauchy model was applied. The Cauchy model in combination with the exponential absorption law, simulates the effect of scattering more successfully than the Tauc-Lorentz model which is not able to account for optical losses below the band-gap. For characterisation of this sample reflectance and transmittance measurements in the range 400–900 nm (where scattering is lower than 1%) were used. The other samples did not present significant scattering.

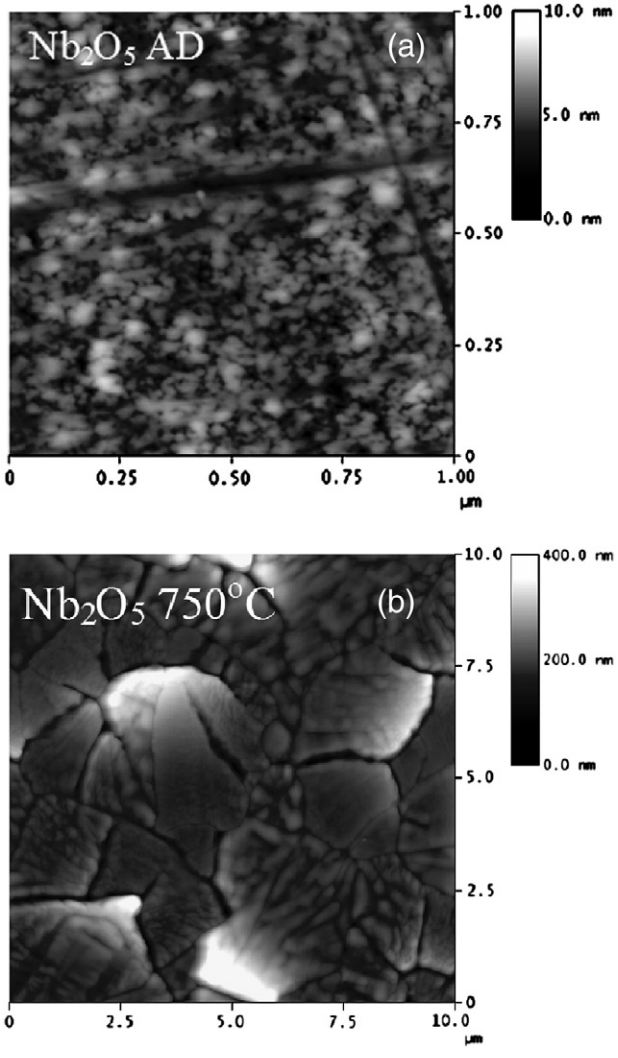

Fig. 6. AFM pictures of an Nb_2O_5 sample prepared on Suprasil substrate AD (a) and annealed at 750 °C (b).

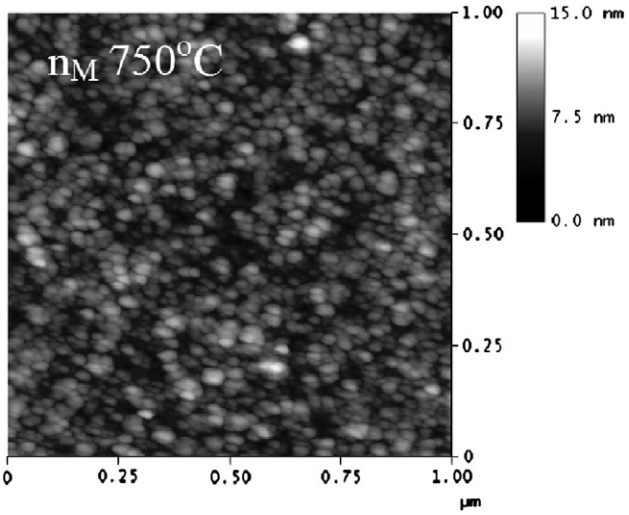

Fig. 7. AFM picture of an n_M sample prepared on a Suprasil substrate annealed at 750 °C.

The thicknesses obtained from optical characterisation (Table 2) are higher than those calculated from deposition rates (Table 1) possibly because of higher porosity, but also due to changes in the deposition conditions from one process to another. Indeed, comparing the differences of thicknesses calculated from $r(t)$ and those obtained from optical characterisation, it is possible to see that greater differences correspond to the AD samples with a higher water content (see Fig. 4); this is related to porosity. Thickness is reduced with increasing annealing temperature: around 7% upon annealing at 500 °C and around 10% upon annealing at 750 °C. Refractive indices increase with temperature: around 0.9% for n_M and n_{M-x} samples annealed at 500 °C and 5% after treatment at 750 °C. For the rest of the mixture layers the increase is around half the value for the samples with high Nb_2O_5 content. This behaviour of the indices and thicknesses indicates that the density of the layers increases with annealing.

The dispersion curves of the AD mixtures match the theoretical LL dispersion curves very well (Fig. 2). The highest discrepancy from the curves is for the n_{M-x} and n_{m+x} samples. The refractive indices at 570 nm as a function of $f_v(SiO_2)$ are shown in Fig. 10, together with the theoretical values calculated from the LL and LIN models. The BG and MG models show nearly the same values as the LIN model. Due to the lack of experimental data for 750 °C annealed Nb_2O_5, the approximate value 2.41 reported in the literature [29], and was used for the simulations. It is clear that the refractive indices of the samples follow the LL and not the LIN model, confirming the appropriateness of application of the LL model in optical characterisation. This is valid for both, AD and annealed samples, in contrast to the expectations that after thermal treatment the mixtures should separate into phases and should be best described by the BG EMT (similar to LIN).

The FTIR spectra of the AD samples (Fig. 3) show an increase in intensity of the bands at 1080 cm^{-1} and 804 cm^{-1} with an increased content of SiO_2. The band assigned to the Si–O–Nb bonds (around 920–930 cm^{-1}) is especially pronounced for the n_m and n_{m+x} samples. The existence of this band suggests that SiO_2 and Nb_2O_5 are mixed at the atomic level, with no significant separation of phases.

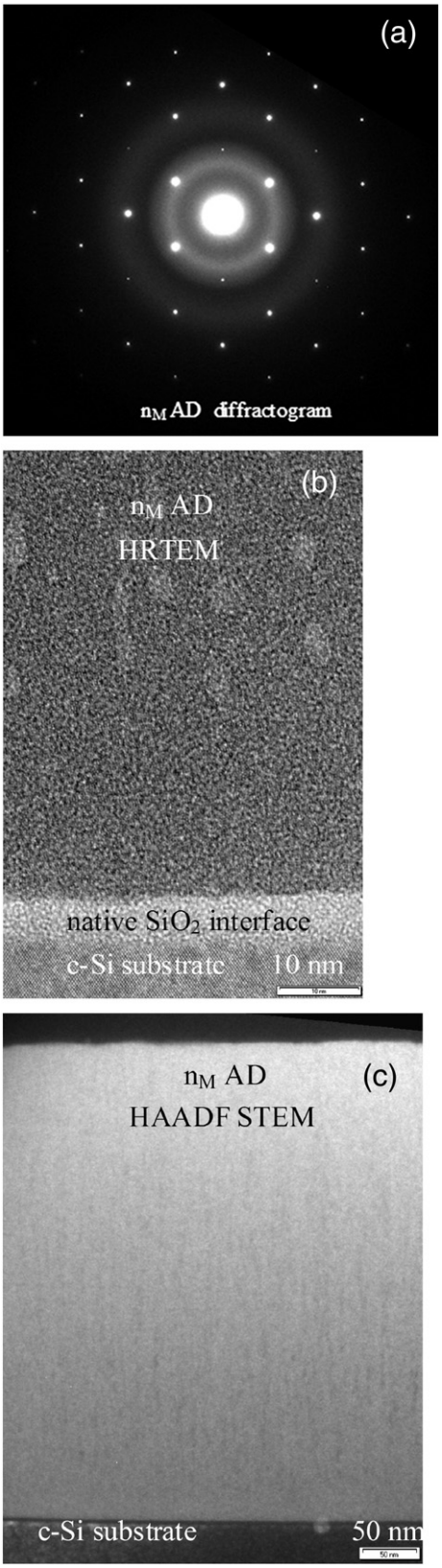

Fig. 8. SAED (a), HRTEM (b) and HAADF STEM (c) images of an AD n_M sample deposited on a silicon wafer chunk.

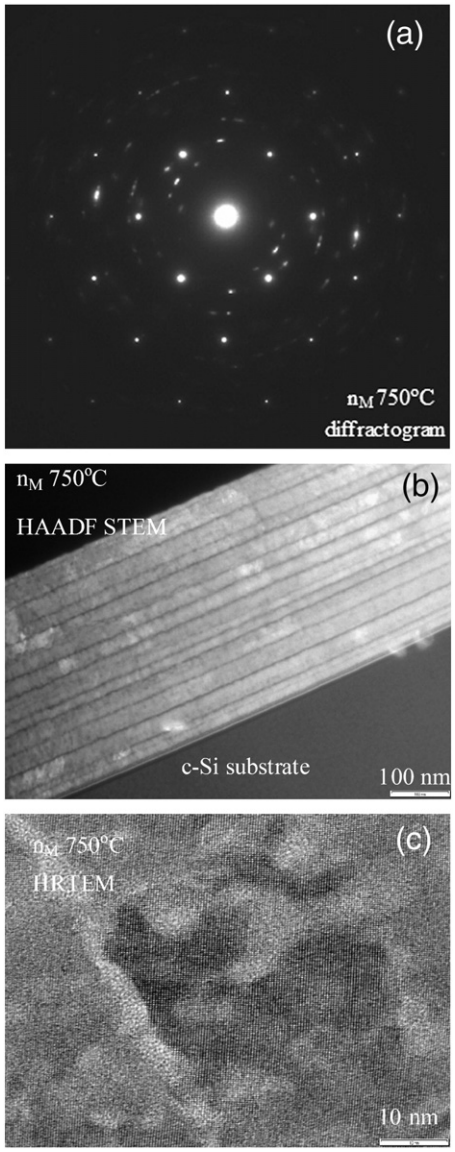

Fig. 9. SAED (a), HAADF STEM (b) and HRTEM (c) images of an n_M sample deposited on a silicon wafer chunk annealed at 750 °C.

The change of intensity of these peaks with temperature indicates breaking of the Si–O–Nb bonds followed by creation of Si–O–Si bonds (increase of the band at 1080 cm^{-1}). Thus, separation of phases occurs during temperature treatment. However, these bands remain visible even after annealing at 750 °C (Fig. 3, sample n_m) suggesting that the process is not completed. The increase of the Si–O–Si band in the Nb_2O_5 sample is attributed to the growth of the native SiO_2 layer at the interface with the Si substrate due to annealing.

Water absorption bands show that all the AD samples have pores filled with water molecules or that water is adsorbed on the surface of the coating (Fig. 4). In FTIR spectra measured three days after annealing at 500 °C (no change in spectra was noticed after three days) these bands are significantly reduced or even absent. Upon annealing at 750 °C, none of the samples shows water absorption. The reduction of thickness found by optical characterisation could be related to the reduction of pore concentration in the layer. Indeed, the area under the water absorption peak is correlated with the shrinking of the thickness. However, the samples after thermal treatment at 500 °C already display no water absorption bands, but their thickness is reduced by an even higher percentage when annealed at 750 °C. This effect cannot be attributed only to restructuring due to crystallisation because it is also observed in samples that did not crystallize. So, although there is no water absorption in the layer (i.e. open voids that can be filled with water molecules), there are still remained closed pores, and thickness can be further reduced by annealing.

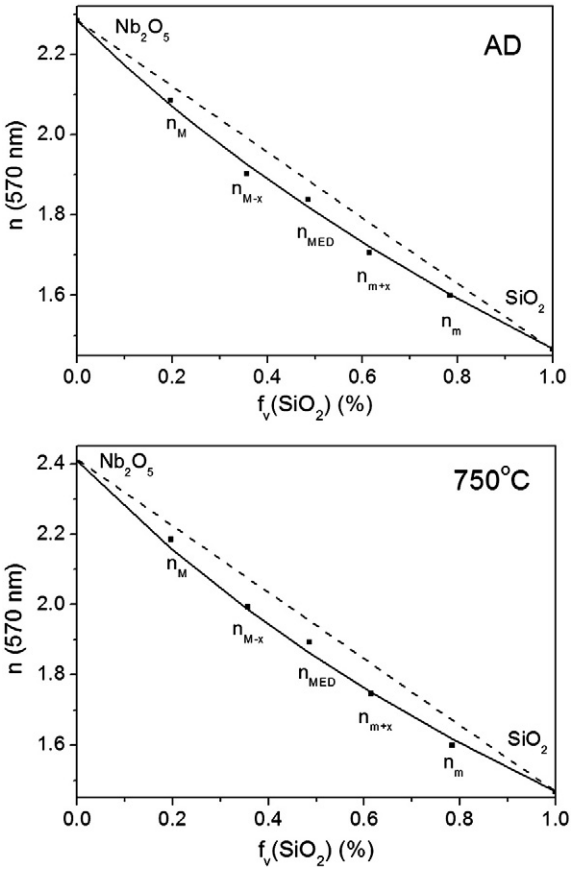

Fig. 10. Refractive indices at wavelength 570 nm of the mixture samples (rectangles), together with theoretical curves for the LL (solid line) and the LIN (dashes) model.

The XRD of the samples annealed at 500 °C show no crystallization. The first crystallisation in the samples appears between 500 °C and 750 °C and only for samples with the highest Nb_2O_5 content ($n_{M\text{-}x}$, n_M and Nb_2O_5) (Fig. 5). The peaks found for $n_{M\text{-}x}$ and n_M correspond to hexagonal crystal structures, while in the case of the Nb_2O_5 sample there is clear splitting of the peaks close to 28.5° and 36.7°, which is characteristic of an orthorhombic structure. The diffractograms of all the other samples present only a halo from the Suprasil substrate and no diffraction pattern is distinguishable. The lack of defined XRD peaks indicates that Nb_2O_5 species are well dispersed in silica (and vice versa) as crystallites are smaller than 2–3 nm (detection limit), or they are present as an amorphous phase.

RMS roughness obtained from XRD analysis (Table 3) does not present any increase of roughness upon annealing for the mixture samples that crystallized (n_M, $n_{M\text{-}x}$). It indicates that no large grains are formed on the surface. On the contrary, RMS roughness shows smoothing of the surface for these samples. It must be noted that it is not expected that the method is precise enough for this level of roughness, but the trend should be correct. For the same samples density also increases after annealing, which is in accordance with the decrease in thickness and lower water absorption found by optical characterisation and FTIR measurements. However, for the Nb_2O_5 sample, RMS was significantly increased. This is related to the formation of large crystalline grains that make a major contribution to the scattering of this sample.

Indeed, RMS values obtained from AFM measurements (Table 3) confirm large grains on the surface of the Nb_2O_5 sample (Fig. 6). The difference in RMS values of the two techniques for this sample may be due to the scale at which the measurements were performed. The RMS values obtained from XRD and AFM measurements are qualitatively in accordance with the level of scattering found in the annealed mixture samples.

SAED patterns of AD Nb_2O_5 (not shown) and n_M samples (Fig. 8) confirm the amorphous structure found by XRD. The spots come from reflections from the Si crystalline structure of the substrate, while rings indicate an amorphous structure of the layer. In the HRTEM image it is possible to see 4–7 nm of SiO_2 layer at the interface between the substrate and the coating, which is the previously mentioned native film growing on Si exposed to the atmosphere. It is possible to see that the structure of the layers is porous, which again is in accordance with FTIR results. Pores are elongated from the bottom to the top of the coating. In initial growth there are no pores. The thickness of the coatings for the Nb_2O_5 and n_M AD samples found by TEM are 450 ± 20 nm, which corresponds to the results of optical characterisation.

The diffractogram of the n_M sample annealed at 750 °C (Fig. 9) shows that the layer is well crystallized, as expected from the XRD results. There is no preferable orientation of the structure in relation to the Si substrate (no overlap with Si substrate reflections). The Z-contrast image demonstrates that the sample is a multilayered film of total thickness 400 ± 20 nm, again in agreement with the thickness from the optical characterisation. The native SiO_2 layer has approximately doubled its thickness with annealing. This is related to the development of an FTIR Si-O-Si band in the Nb_2O_5 sample. The Z-contrast image indicates that 10–30 nm thick layers consist of an element with high atomic number (Nb). They are separated by layers of 1–3 nm of a light element (Si). Although the layered structure demonstrates separation of the mixture into phases, the HRTEM images show that they are not well defined. This can be related to the FTIR results which indicate that Si-O-Nb bands of some samples remain detectable even after annealing at 750 °C, and that the process of separation into phases is not completed. Also, this can be correlated with the optical characterisation results showing that refractive indices of the mixtures are best described by the LL EMT even upon annealing. Indeed, the limits of phase size for BG and MG theory to become effective is 3–30 nm [20] (visible to mid-infrared wavelengths). The uncompleted separation of phases into layers of 1–3 nm is obviously under this limit. Therefore, the LL model should be implemented into the design software to simplify linking design and volume fraction values that should be controlled in the deposition process to obtain the desired refractive index profile.

The multilayer structure of the annealed n_M coating is unexpected. However, it can be related to the previous study [22] presenting periodical regions of higher and lower content of SiO_2 in the mixture coating deposited as a layer of constant refractive index. This periodicity has been related to the rotation of the sample placed at calotte and lateral positions of the evaporation material crucibles indicating that the mixture of materials in the vapour is not uniform in the chamber. The concentration of the corresponding material in the vapour is higher above the crucible. It is possible that during annealing, due to crystallisation, the regions that are poor in one material become even more depleted resulting in a layered structure that is more pronounced than in the AD coating.

6. Conclusions

Results of optical characterisation of Nb_2O_5–SiO_2 mixture samples show that refractive indices of both, as deposited and annealed samples, follow LL EMT. Structural analysis of as deposited samples (FTIR, XRD diffractograms, TEM) shows that the materials are well mixed, at the atomic level (Si–O–Nb bonds). There is no separation into phases for these samples, which is a condition for the validity of the LL EMT. The materials in the mixture layers show phase separation and crystallisation after annealing (FTIR, XRD, TEM, AFM, scattering). The process of separation remains incomplete and the size of the phase grains insufficient after annealing at 750 °C for the BG or LIN

EMT to become effective for electron beam deposited Nb_2O_5–SiO_2 mixtures (FTIR, HRTEM). Thus, the LL EMT has been shown to be the most appropriate model for Nb_2O_5–SiO_2 mixtures both by optical characterisation and by relating optical parameters of the mixtures to the structure of the mixtures. The LL EMT should be taken into consideration when developing algorithms for the design of gradient index coatings to simplify the transition from design to the corresponding deposition process.

Acknowledgements

Special thanks to Olaf Stenzel for support and advice. The authors thank Heidi Haase for technical assistance and Sabine Grözinger for TEM sample preparation. Vesna Janicki wishes to thank the Fraunhofer Society in Germany for a Fraunhofer Fellowship at IOF in Jena.

References

[1] W.H. Southwell, J. Opt. Soc. Am. A 5 (1988) 1558.
[2] T.D. Rahmlow Jr., J.E. Lazo-Wasem, Proc. SPIE 3133 (1997) 25.
[3] P.G. Verly, J.A. Dobrowolski, Appl. Opt. 29 (1990) 3672.
[4] D. Rats, D. Poitras, J.M. Soro, L. Martinu, J. von Stebut, Surf. Coat. Technol. 111 (1999) 220.
[5] M.-A. Raymond, S. Larouche, O. Zabeida, L. Martinu, J.E. Klemberg-Sapieha, Proc. 44th Ann. Tech. Conf. Soc. of Vacuum Coaters, 2001, p. 301.
[6] R. Vernhes, O. Zabeida, J.E. Klemberg-Sapieha, L. Martinu, Appl. Opt. 43 (2004) 97.
[7] D. Ristau, H. Schink, F. Mittendorf, J. Akhtar, J. Ebert, H. Welling, NIST Spec. Publ. 775 (1988) 414.
[8] D.A. Bruggeman, Ann. Phys. 24 (1935) 636.
[9] L. Lorenz, Ann. Phys. 11 (1880) 70.
[10] J.C. Maxwell Garnett, Philos. Trans. R. Soc. Lond. A 203 (1904) 385.
[11] A.V. Tikhonravov, M.K. Trubetskov, T.V. Amotchkina, M.A. Kokarev, N. Kaiser, O. Stenzel, S. Wilbrandt, D. Gäbler, Appl. Opt. 45 (2006) 1515.
[12] V. Janicki, S. Wilbrandt, O. Stenzel, D. Gäbler, N. Kaiser, A. Tikhonravov, M. Trubetskov, T. Amotchkina, J. Opt. A: Pure Appl. Opt. 7 (2005) L9.
[13] S.W. Wang, X.X. Huang, J.K. Guo, B.S. Li, Mater. Lett. 28 (1996) 43.
[14] N. Özer, M.D. Rubin, C.M. Lampert, Sol. Energy Mater. Sol. Cells 40 (1996) 285.
[15] A. Pawlicka, M. Atik, M.A. Aegerter, Thin Solid Films 301 (1997) 236.
[16] M. Paulis, M. Martín, D.B. Soria, A. Díaz, J.A. Odriozola, M. Montes, Appl. Catal. A 180 (1999) 411.
[17] Powder Diffraction File, Joint Committee on Powder Diffraction Standards, International Centre for Diffraction Data, 1601 Park Lane, Swarthmore, PA 19081, USA, 2004.
[18] H. Szymanowski, O. Zabeida, J.E. Klemberg-Sapieha, L. Martinu, J. Vac. Sci. Technol., A 23 (2) (2005) 241.
[19] M.S.P. Francisco, Y. Gushikem, J. Mater. Chem. 12 (2002) 2552.
[20] G.A. Niklasson, C.G. Granqvist, O. Hunderi, Appl. Opt. 20 (1981) 26.
[21] D.E. Aspnes, Thin Solid Films 89 (1982) 249.
[22] R. Leitl, O. Stenzel, S. Wilbrandt, D. Gäbler, V. Janicki, N. Kaiser, Thin Solid Films 497 (2006) 135.
[23] V. Janicki, D. Gäbler, S. Wilbrandt, R. Leitel, O. Stenzel, N. Kaiser, M. Lappshies, B. Görtz, D. Ristau, C. Rickers, M. Vergöhl, Appl. Opt. 45 (2006) 7851.
[24] S. Bosch, J. Ferré-Borrull, J. Sancho-Parramon, Solid State Electron. 45 (2001) 703.
[25] J. Tauc, R. Grigorovici, A. Vancu, Phys. Status Solidi A 15 (1966) 627.
[26] G.E. Jellison Jr., F.A. Modine, Appl. Phys. Lett. 69 (1966) 371.
[27] E.B. Pereira, M.M. Pereira, Y.L. Lam, C.A.C. Perez, M. Schmal, Appl. Catal. A 197 (2000) 99.
[28] S. Laux, W. Richter, Appl. Opt. 35 (1996) 97.
[29] J.-P. Masse, H. Szymanowski, O. Zabeida, A. Amassian, J.E. Klemberg-Sapieha, L. Martinu, Thin Solid Films 515 (2006) 1674.